ESD TDR 63-379

63-4

SR-36

THE MITRE CORPORATION
P. O. Box 208
Bedford, Massachusetts

PHOTOELASTIC DETERMINATION OF BOUNDARY STRESSES AROUND TUNNELS OF VARIOUS CROSS-SECTIONAL SHAPES

by

Daniel Post*
Marshall Leitman*
C. C. Mow

21 December 1961

*Rensselaer Polytechnic Institute
Troy, New York

Air Force Contract AF-33(600)39852
Project 600

MITRE STUDIES RELATED TO SURVIVABILITY OF
AIR FORCE COMMAND AND CONTROL SYSTEMS

SR-18, "On the Application of the Theory of Locking Media to Ground Shock Phenomena," M. G. Salvadori, R. Skalak, and P. Weidlinger.

SR-19, "Theoretical Studies on Ground Shock Phenomena," M. L. Baron, H. H. Bleich, and P. Weidlinger.

SR-22, "A Study on the Effect of a Progressing Surface Pressure on a Viscoelastic Half-Space," M. L. Baron, R. Parness, J. L. Sackman, and P. Weidlinger.

SR-26, "A Submersible Emergency Command Control Communication Barge," S. S. Murray.

SR-28, "On the Wave Transmission Between Liquid and Voight Solid," C. C. Mow.

SR-29, "MITRE Seminar on Survivability of Command Control Systems," J. J. O'Sullivan and F. R. Eldridge.

SR-30, "Design of Superhard Command Post, 10,000 psi Water Shaft Concept," Marc Peter.

SR-31, "The Adaptability of Ground Effect Machines and Existing Ground Vehicles," Guy B. Panero, Engineers.

SR-33, "Design Study for a Superhard Shallow Buried Emergency Command Post," E. Cohen and G. Pecone.

SR-34, "Soft Filled Liners for Rock Tunnels in Very High Pressure Environments," Newmark, Hansen and Associates.

SR-36, "Photoelastic Determination of Boundary Stresses Around Tunnels of Various Cross-Sectional Shapes," Daniel Post, Marshall Leitman, and C. C. Mow.

SR-37, "An Experimental Study of Cavity Collapse Mechanism," Lewis T. Assini, John K. Hawley, and C. C. Mow.

SR-39, "The Feasibility of a Radiation Protected Communications Repair Vehicle," T. W. Schwenke, N. J. Donnelly, W. W. Hicks, and B. A. Frances.

TABLE OF CONTENTS

ILLUSTRATIONS

ABSTRACT

Numerical values of static stress concentration factor for ten typical tunnel cross-sections, determined by the methods of photo-elasticity are presented herein. Results indicate that stress distribution around a cavity are very sensitive to its cross-section's configuration and the direction of the applied load. The values of the stress concentration factors for the configuration considered ranges from 3.24 - 6.10 for maximum compressive stress and ranged from 1.07 - 2.18 for the maximum tensile stress.

1. OBJECTIVE

It was desired to obtain the elastic solution of boundary stresses developed in deep tunnels under uniform uniaxial load. The study is limited to elastic, homogeneous materials. Ten prescribed tunnel configurations were investigated.

2. INTRODUCTION

Recent studies concerning the feasibility of deep underground command and control installations have indicated that a cavity located under three to four thousand feet of overburden could withstand the shock due to the direct hit of a multi-megaton weapon. This conclusion is based on the extrapolation to depth of the free-field stresses in the close-in region where a hydrodynamic analysis is valid.[1] However, the survivability of a deep underground cavity depends not only on the magnitude of the free-field stress but also on geometric configuration of the cavity itself.

Baron, et al[2] have investigated the diffraction effects of a circular cavity in an elastic half-space, and have shown that there is a maximum dynamic stress magnification of approximately 3.3; the corresponding static stress magnification being 3., ARF has conducted[3] a photo-elastic study where the dynamic stress concentration factors for circular, elliptical and square (with filleted corners) holes are determined. It was found that the difference between the maximum static and maximum dynamic stress is of the order of 10-20%.

In view of this apparent static-dynamic similitude and since the static photo-elastic analyses are much easier to carry out, it was felt that a static photo-elastic investigation of the boundary stresses associated with several typical cavity cross-sections was warranted. This report presents the results of such an investigation.

3. EXPERIMENTAL APPROACH

The elasticity problem of a long tunnel of constant cross-section, subjected to uniform loading along its length is in the category of plane strain. It is shown in the Theory of Elasticity that the stress distribution developed in planes of the cross-section, i.e., in planes normal to the axis of the tunnel, is identical to that developed in

the equivalent plane-stress system. Thus, thin models were employed in which the tunnel dimensions were large compared to the model thickness.

While the loading system of interest is uniaxial compression, the system employed in these tests was uniaxial tension. It is clear that the distribution of stresses in the small strain elasticity solution is independent of the sign of applied load. The boundary stresses shown in the accompanying graphs are for tensile loads; to convert to the equivalent system of compressive loads, interchange symbols for tensile and compression stress.

Ideally, a deep tunnel in a continuous medium should be represented by a model whose overall width is large compared to the tunnel width. As a practical compromise, a ratio of 4:1 was chosen; with these proportions, the proximity of the free edges of the model have little influence on the stress distribution on the tunnel boundary.

The photoelastic method was chosen for the investigation of these irregular tunnel cross-sectional shapes, rather than the analytical method of elasticity. Since the boundary shapes could be produced mechanically but could not be satisfactorily prescribed by a mathematical equation, the experimental method was by far the easier of the two alternatives.

Photoelasticity is based upon a unique property of certain transparent materials, notably some plastics. When a ray of light enters a stressed photoelastic model, it divides into two plane polarized components, with directions of polarization parallel to the directions of principal stresses. In addition, each component propagates through the model material with a velocity that depends upon the state of stress, and the two components emerge out of phase with each other. The components are recombined in the photoelastic polariscope to exhibit constructive or destructive interference, according to the phase difference. In this way, a continuous pattern of optical interference fringes (or bands) is produced throughout the field of view. The phase difference at any point in the model can be determined from the interference pattern, and from this, information relating to the state of stress at any point is obtained.

The phase difference, or in more common terminology, the photoelastic fringe order, is proportional to the difference of principal stresses developed at each point in the model. At free boundary points, e.g., the tunnel boundaries in these analyses, the principal stress normal to the boundary must be zero, and the fringe order is directly proportional to the tangential boundary stress. Thus, boundary stress distribution is given by the graph of fringe order vs. position along the boundary.

4. MODEL AND LOADING SYSTEM

A commercial plastic, Homolite 100, was selected as the model material. It exhibits high stress-optical sensitivity and other desirable photoelastic properties. It is available in large sheets as a colorless, homogeneous plastic with glass-like surfaces.

Model dimensions were 10" width, 40" length, 3/16" thickness, with 2 1/2" tunnel width. Tunnel configurations are given in Table I. Loads were applied by means of four-arm whipple-trees as illustrated in Fig. 1. Well machined whipple-trees were employed to produce a uniform load across the plate without introducing any transverse constraints; their effectiveness is evidenced by the striking symmetry of the photoelastic patterns shown in succeeding figures.

The applied tensile loads were not measured. Instead, a self-indicating technique was used in which measurements were taken in a region where the relationship between stress and load was the same for all specimens. For increased accuracy, a stress concentration in the form of a small hole (3/4" diameter) was introduced midway between the tunnel and whipple-tree and the maximum fringe order at the hole boundary was observed in each test. This data permitted direct correlation between models on the basis of a common tensile load.

5. PHOTOELASTIC POLARISCOPE

A diffuse light doubling polariscope was employed, as illustrated in Fig. 1. In this system, a mirror placed immediately behind the model returns the light rays for a second passage through the model, thus doubling the phase difference and doubling the sensitivity of the experiment. Light-field circular polarization was employed; in order to eliminate the influence of

polarization by the beam-splitter, the polarizer axis was vertical, the analyzer axis horizontal, and the quarter-wave plate axes 45^{o} from the vertical. A sodium vapor lamp was used as the monochromatic light source. The camera was equipped with a 20" focal length lens and a Polaroid-Land camera back; Polaroid film yielding positive transparencies was used.

The entire polariscope was mounted on an elevator pedestal so that photographs of the tunnel and reference hole could be taken in sequence.

6. EXPERIMENTAL PROCEDURE

The optical system was aligned by optical reflection techniques to position the planes of the model and mirror perpendicular to the axis of the camera. The camera was focused on the plane of the model.

For each tunnel shape, the photoelastic model was machined by means of a high speed routing machine equipped to follow a previously prepared metal template of the model contours. Tungsten carbide tools were used. A jet of compress air was played on the tool for cooling and chip removal.

The model was cleaned and installed in the loading frame without delay. A deleterious time-edge effect gradually develops in the model material upon exposure of freshly cut surfaces to the atmoshere, but this remains inconsequential if the experiment is performed rapidly. The tensile load was increased until the photoelastic fringe order at the most highly stressed point was approximately twelve.

The photoelastic pattern surrounding the tunnel was photographed. The optical system was then raised to the level of the reference hole and this photoelastic pattern was photographed.

Positive photographic prints were produced for each tunnel pattern as shown in Figs. 2 through 11.

The fringe orders along the tunnel boundaries were ascertained, and divided in each case by the maximum fringe order at the reference hole. This dimensionless ratio was plotted to such a scale that the maximum stress developed in the case of the circular tunnel, Fig. 2, would equal $3.24\sigma_o$. Here, σ_o represents the tensile load divided by the gross cross-sectional area (10" x 3/16") of the plate; alternatively, σ_o represents the tensile stress that would have existed in the region of the tunnel if the tunnel was not present. The factor 3.24 is the

known stress concentration factor* for a circular hole in a finite tensile plate of these proportions, when based upon the gross cross-sectional area. Thus, the graphs shown in Figs. 11 through 21 are unified on the basis of a common applied stress.

7. RESULTS

The results of the investigation are presented in graphical form in Figs. 12 through 21. In each case the magnitude of stress at any boundary point is given by the length of the generatrix normal to the boundary.

Peak tensile and compressive stresses are given in numerical form on the graphs and also in Table II.

The limit of experimental error is estimated as $\pm 1/4$ of a fringe order. Maximum fringe order at the reference hole averaged 7 for all tests, yielding a representative maximum error of approximately $\pm 4\%$ in unifying the data on the basis of a common load. Maximum fringe order at the tunnel boundary averaged approximately 10, yielding a representative maximum error of ± 2 1/2% of the maximum stress. Accordingly, the accuracy of individual stress distributions shown in the graphs is estimated to be within ± 2 1/2% of peak stress, while the accuracy of corresponding numerical values is within ± 6 1/2%.

The results represent the effect of uniaxial loading applied in the direction of the vertical axis of symmetry for tunnel Models 1 through 9. In the case of Model 10, the uniaxial loading was applied at an angle of 30° from the axis of symmetry.

8. CONCLUSION

Observing the result obtained herein, one would recommend strongly that, tunnel shapes shown in Figures 12, 13, 15, 16, 18, and 20 be used for any future underground command and control installation, or in general it is preferred that the axis of the tunnel which lies in the direction of loading be larger than the axis that is perpendicular to the line of loading.

Another very interesting and perhaps very important result obtained in this report is the extreme sensitivity of the stresses around the cavity due to a change of direction of loading. This is shown in Figure 21 which

*Peterson, R. E., Stress Concentration Design Factors, John Wiley and Sons, Inc., New York, 1953.

has the same cross-section as Figure 13 except the load is applied at 30^{o} to its axis of symmetry. In the case of 21, it is found that maximum compressive stress is 5.10 and maximum tensile stress is 2.18 as compared with 3.24 and 1.26 in Figure 13. Therefore, great care must be exercised in choosing the tunnel configuration so that all factors are to be incorporated. Ideally, one should choose the circular cross-section so that the axis of symmetry will be preserved in all directions.

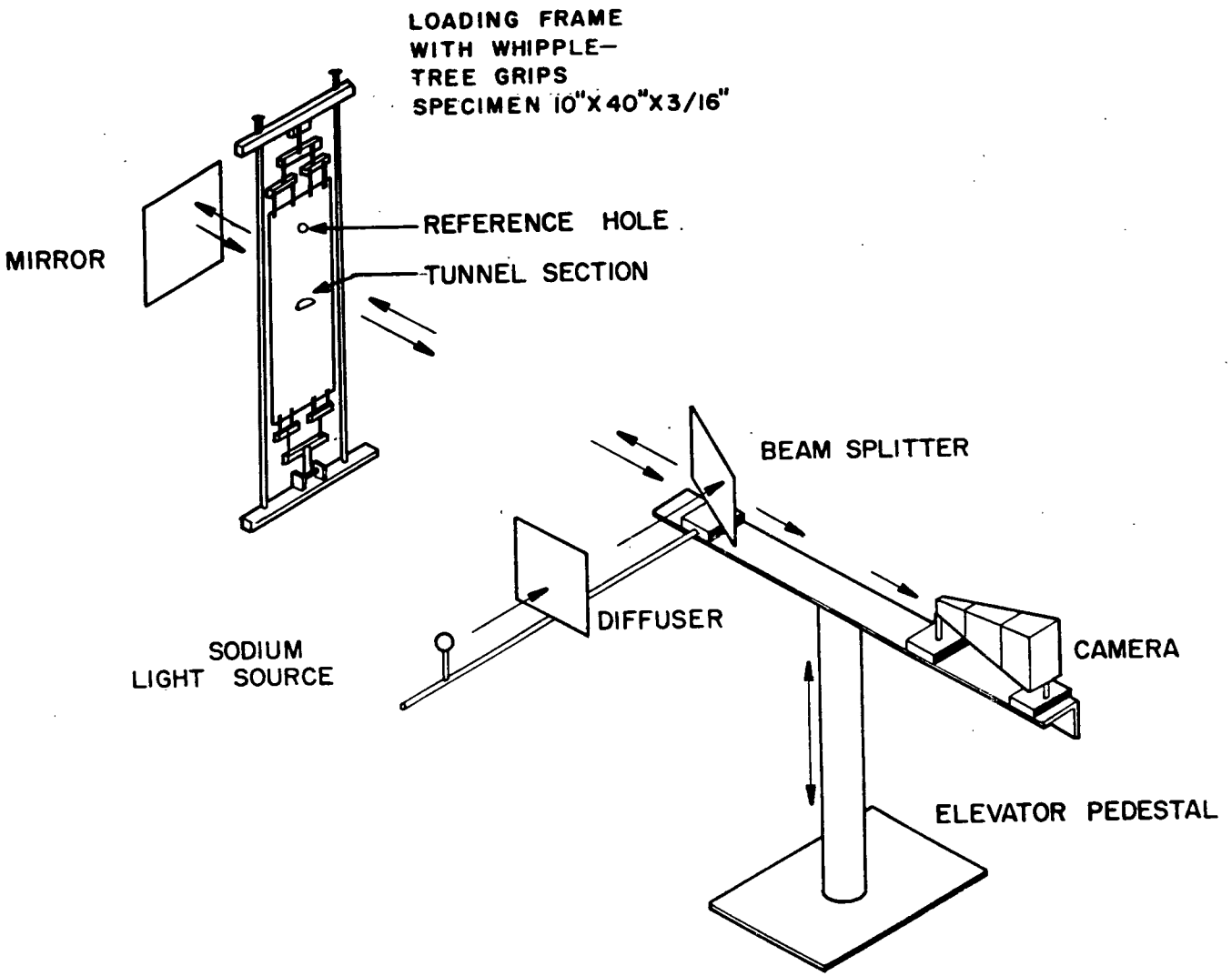
LOADING FRAME
WITH WHIPPLE–
TREE GRIPS
SPECIMEN 10"X40"X3/16"
MIRROR
REFERENCE HOLE
TUNNEL SECTION
BEAM SPLITTER
DIFFUSER
SODIUM
LIGHT SOURCE
CAMERA
ELEVATOR PEDESTAL

FIG. I-A

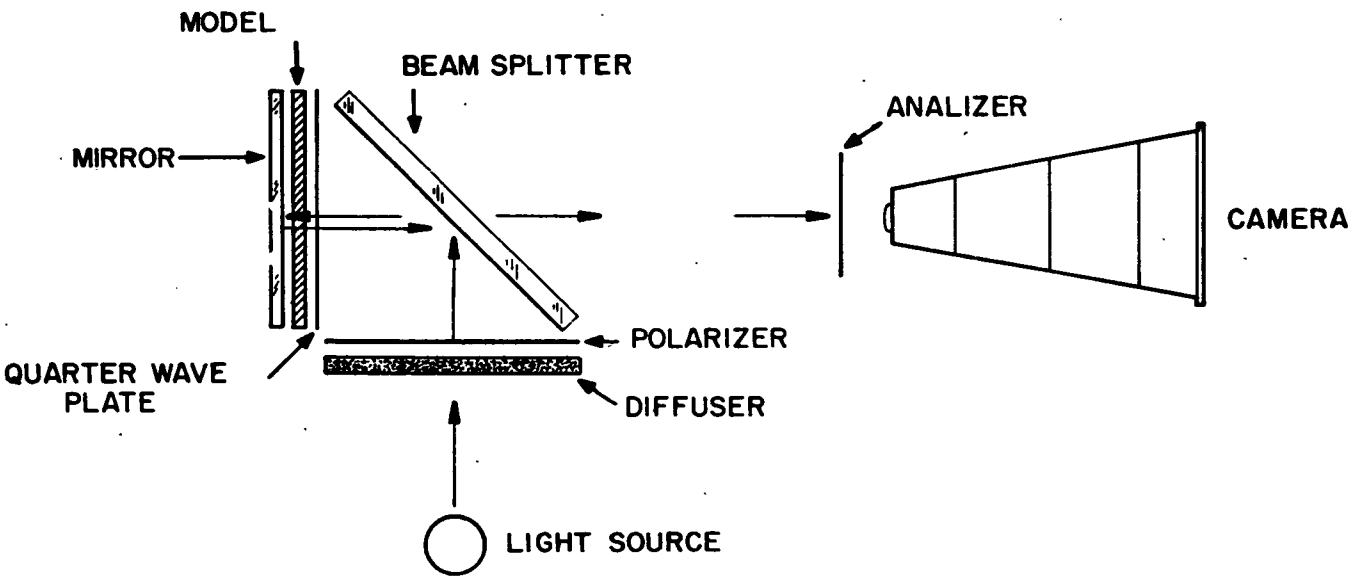
MODEL
BEAM SPLITTER
ANALIZER
MIRROR
CAMERA
POLARIZER
QUARTER WAVE PLATE
DIFFUSER
LIGHT SOURCE

FIG. I- B

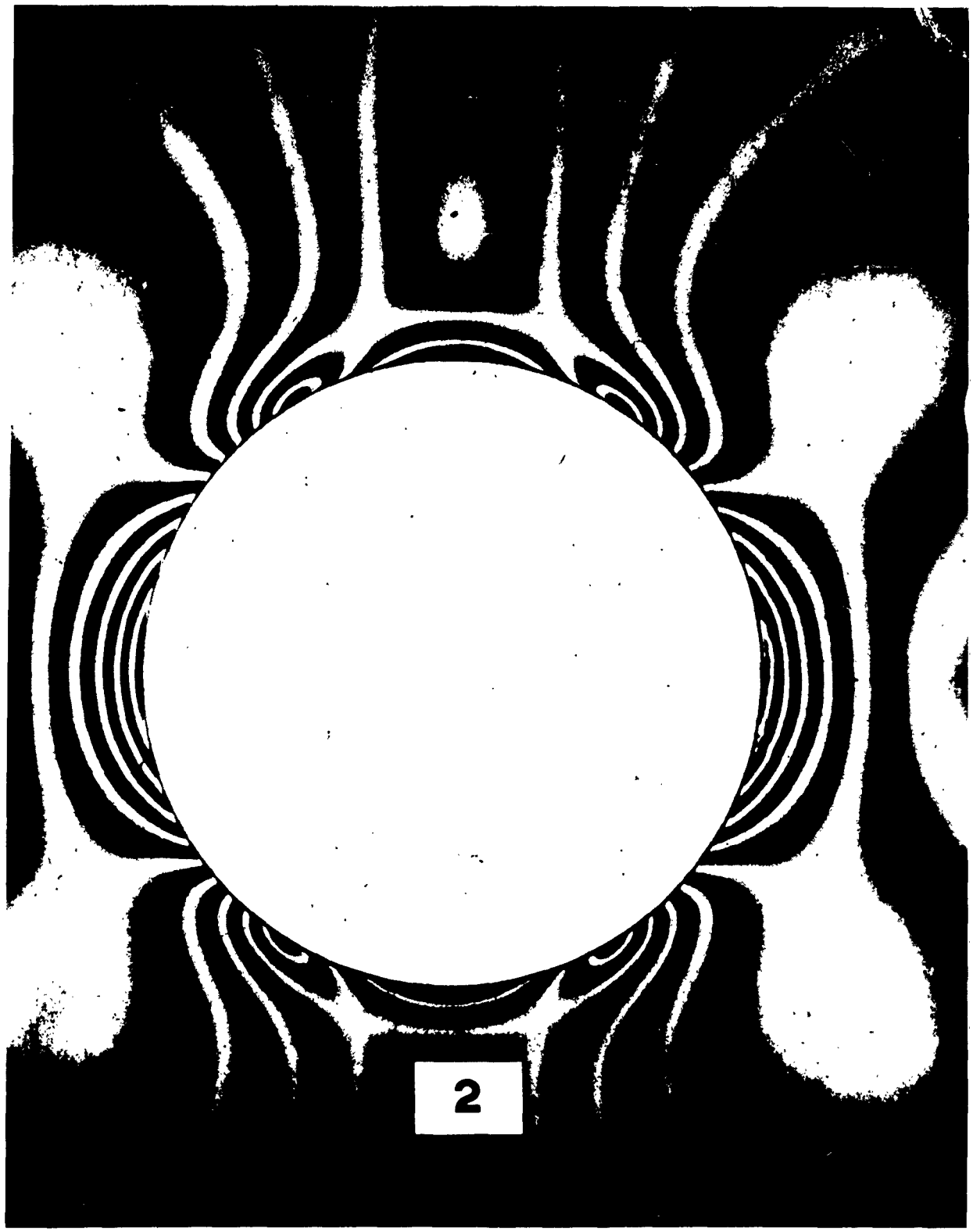
2

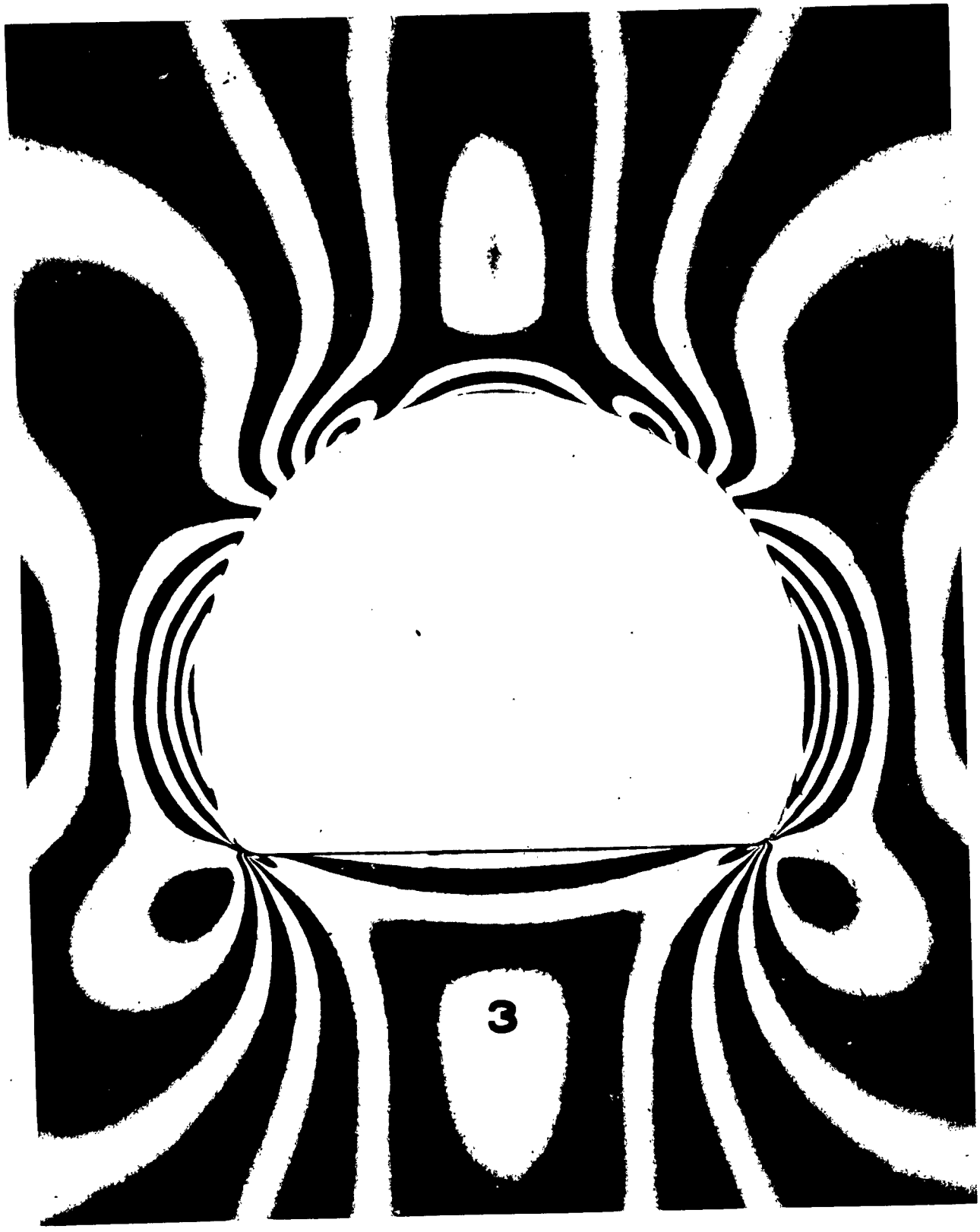
3


4

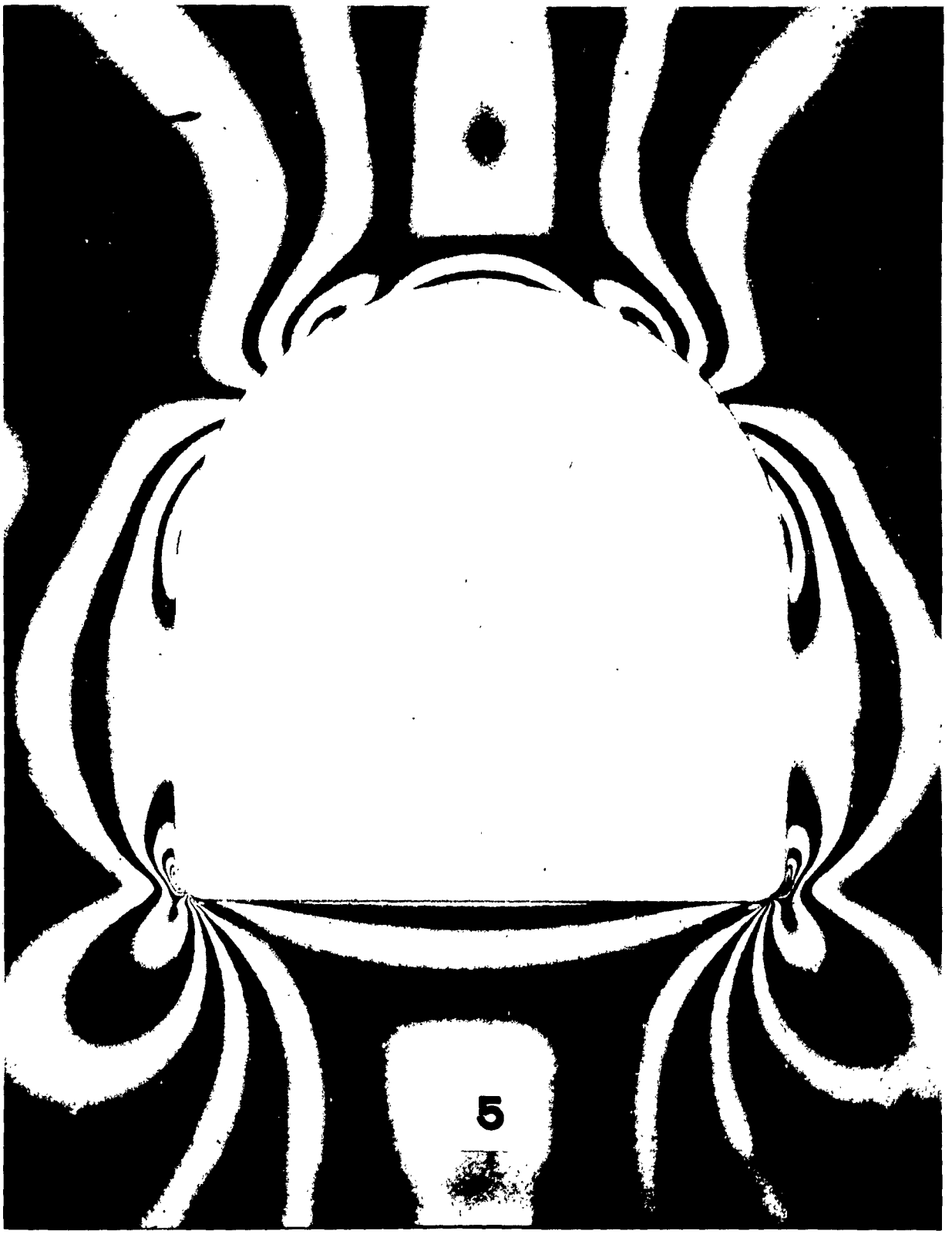
5

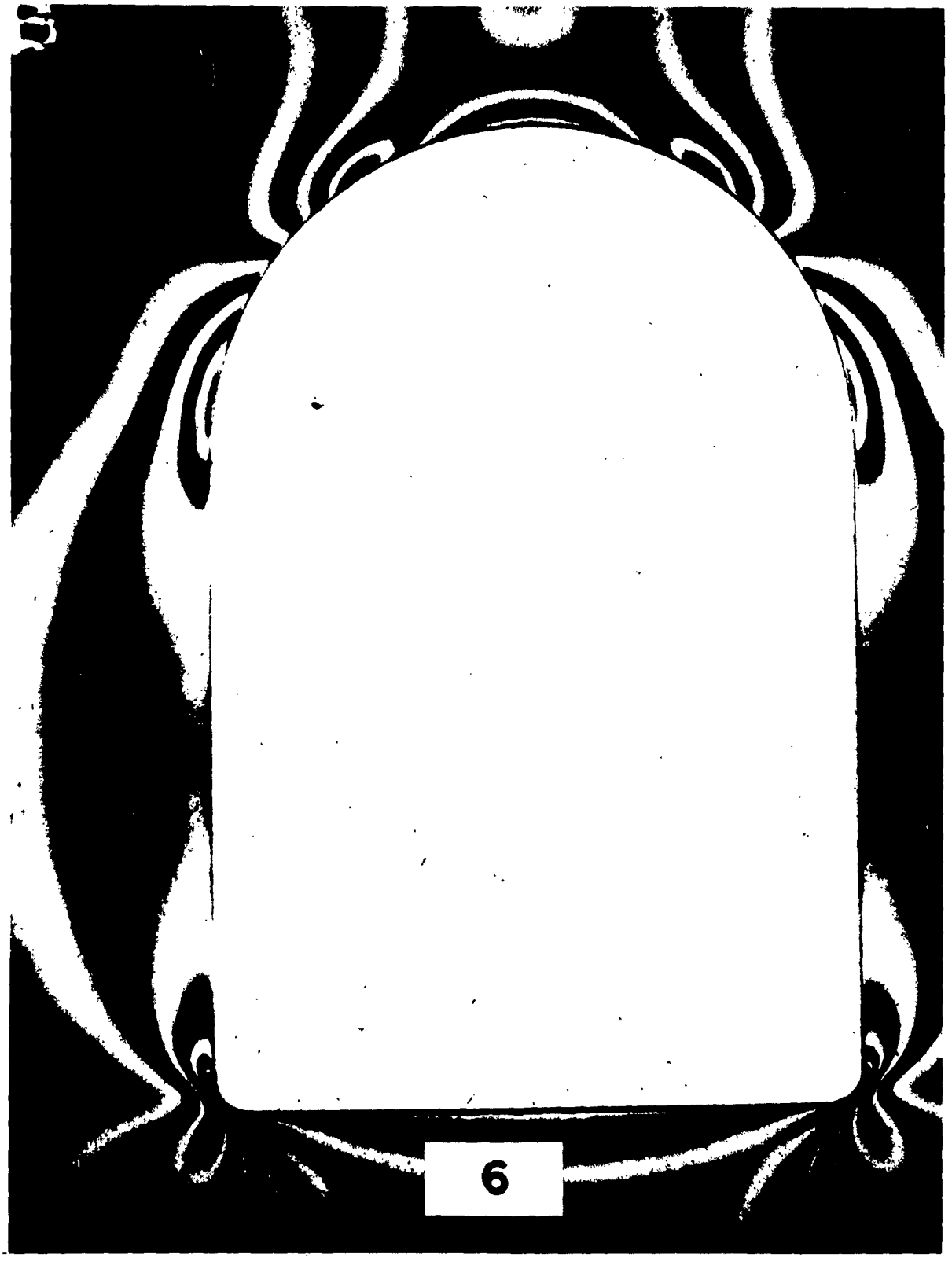
6

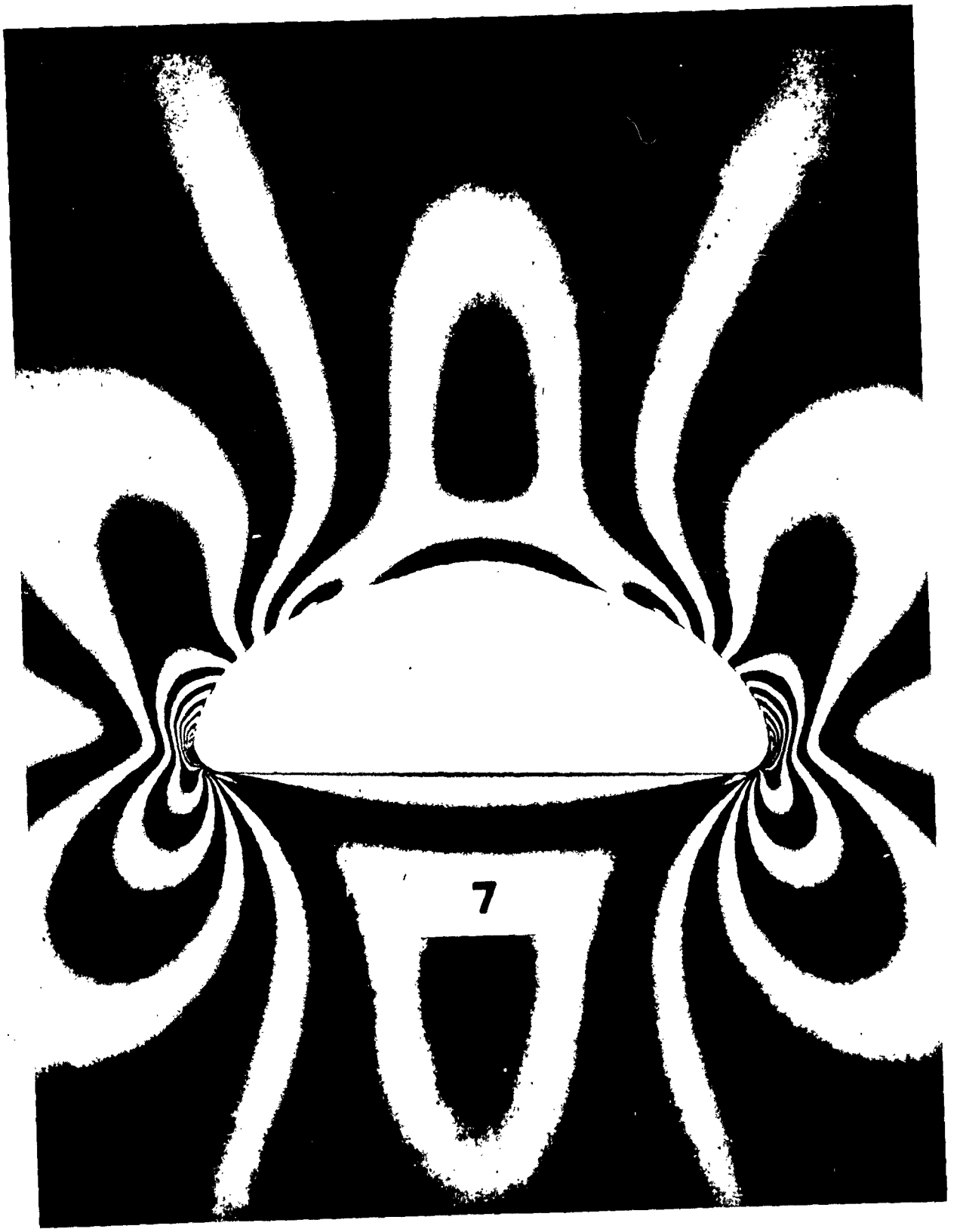
7

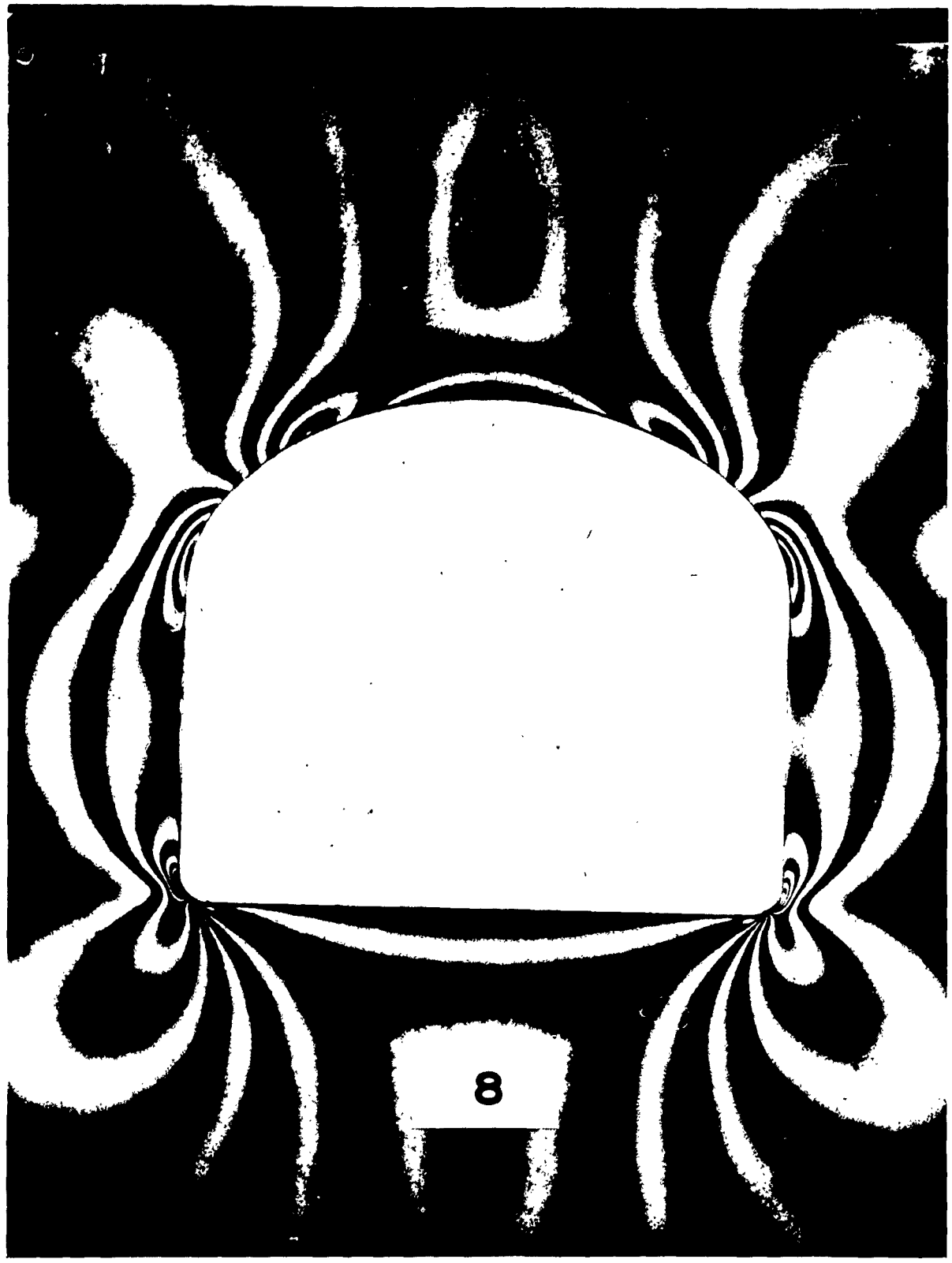
8

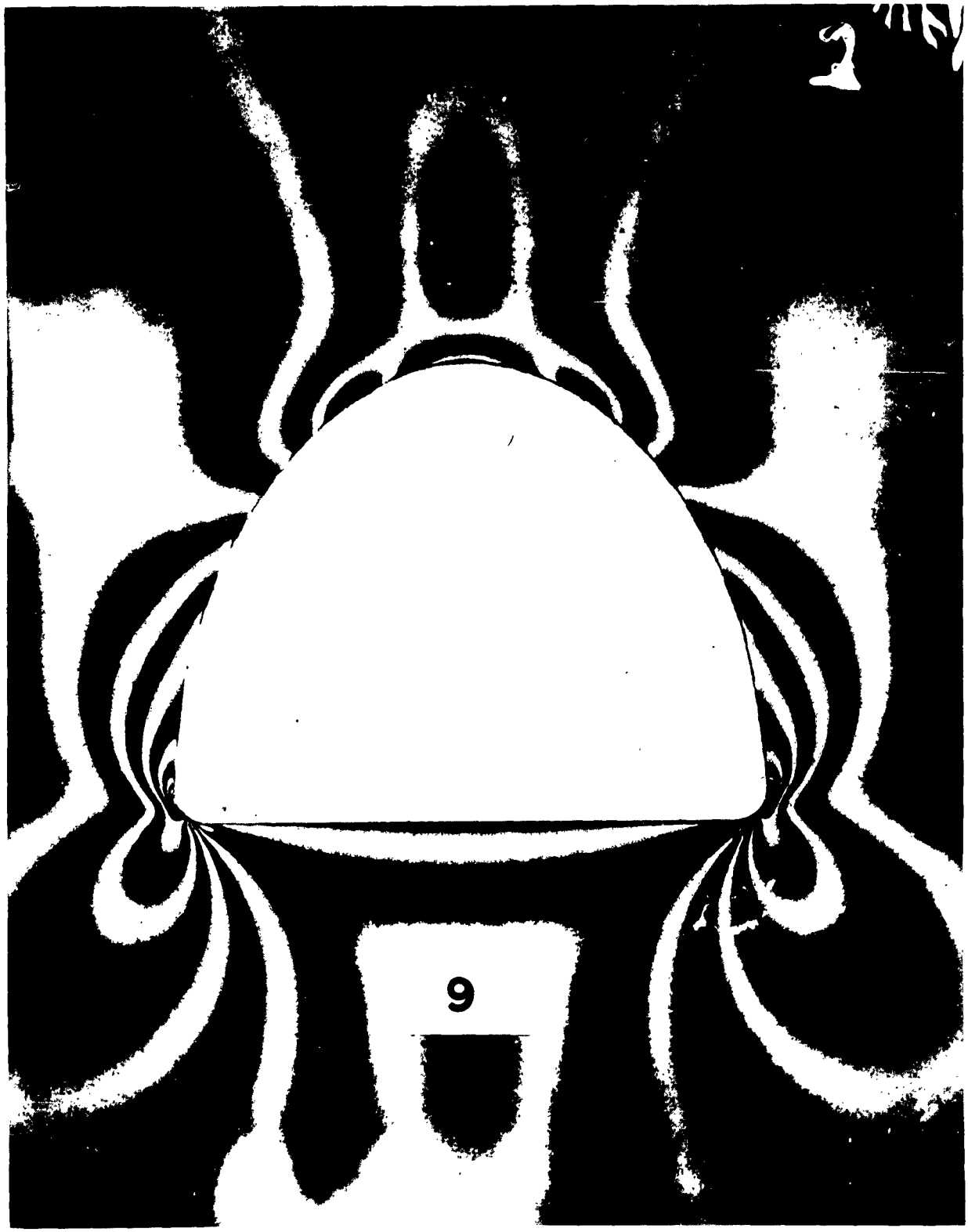
9

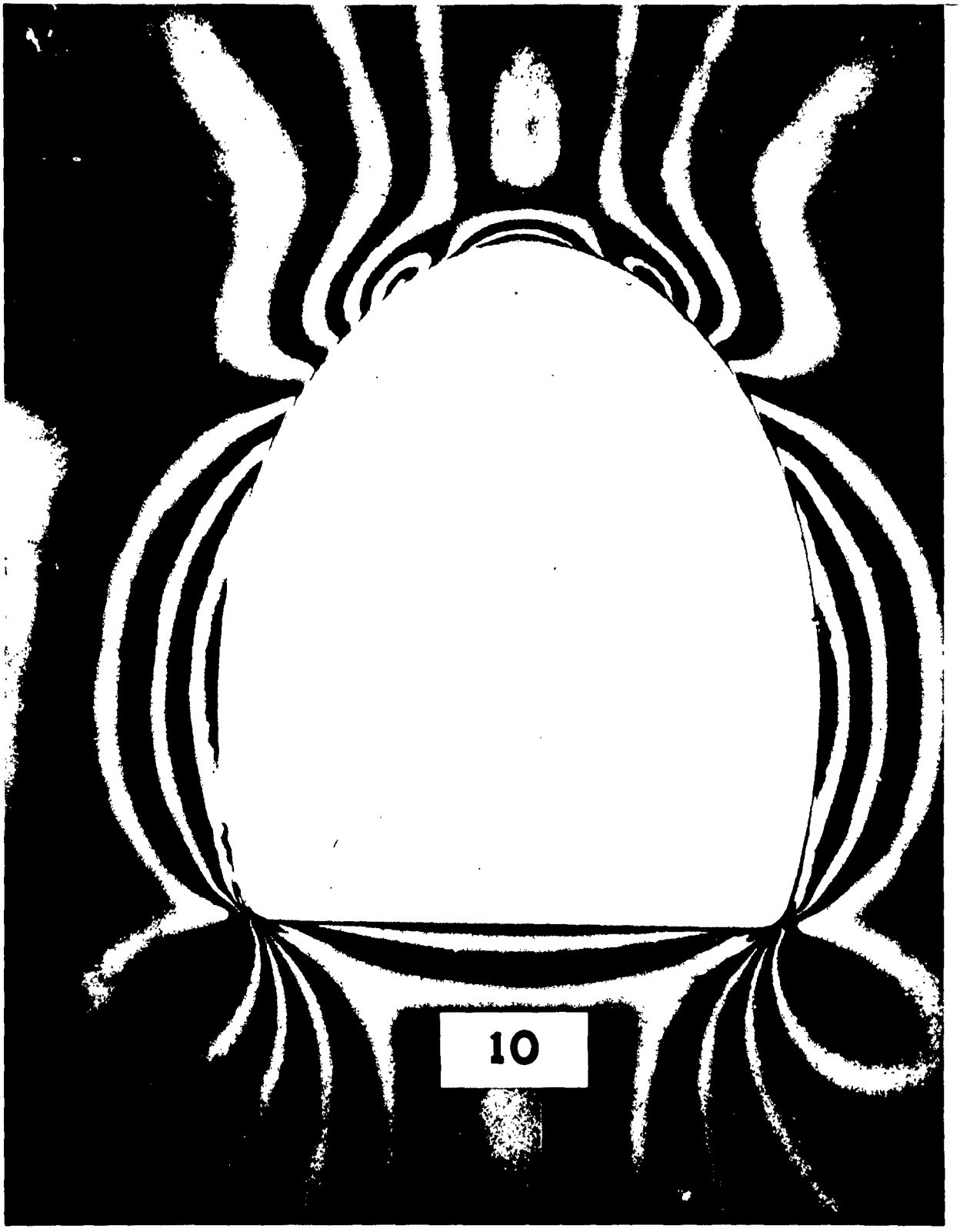
10

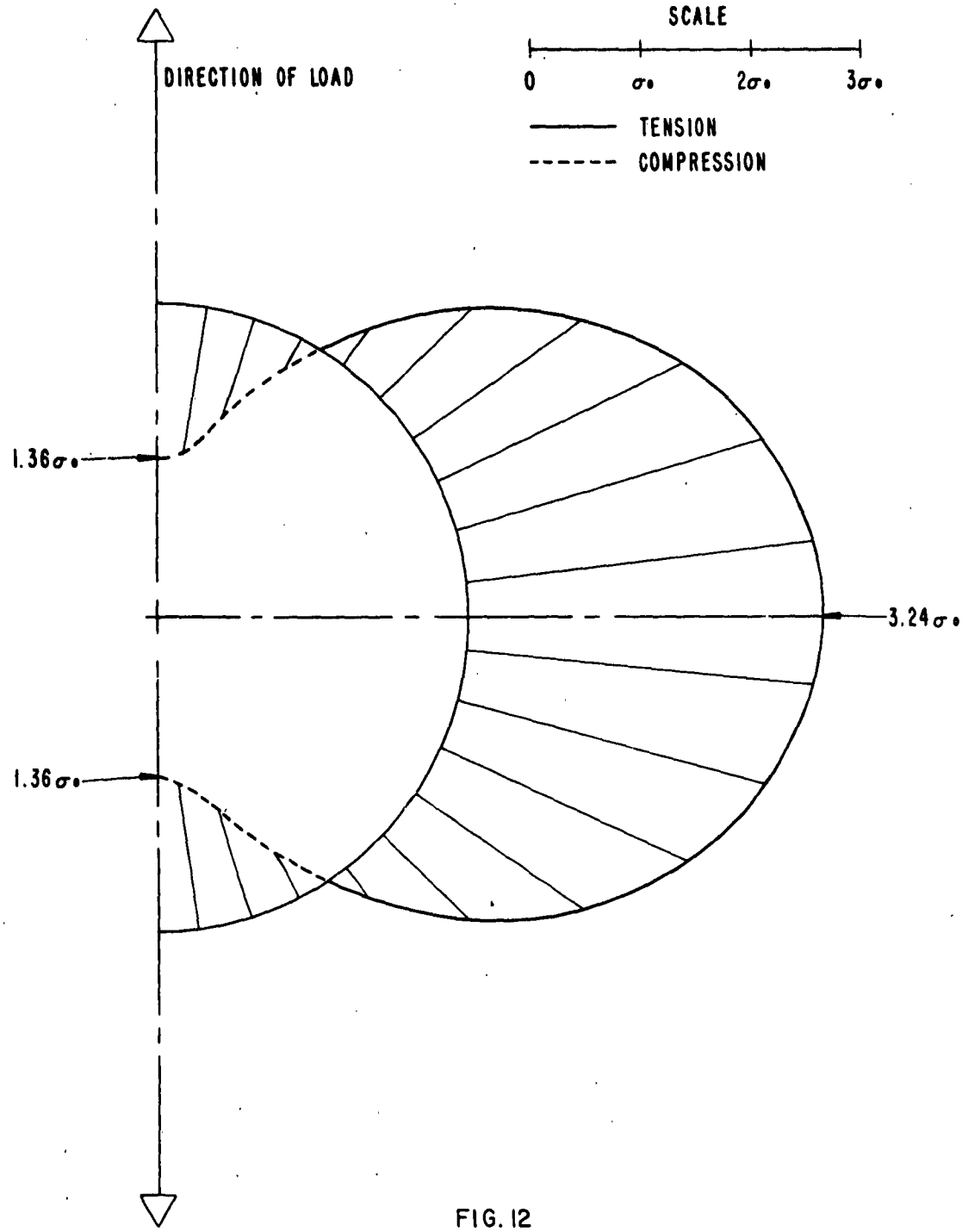

FIG. 12
MODEL I

IA-6707

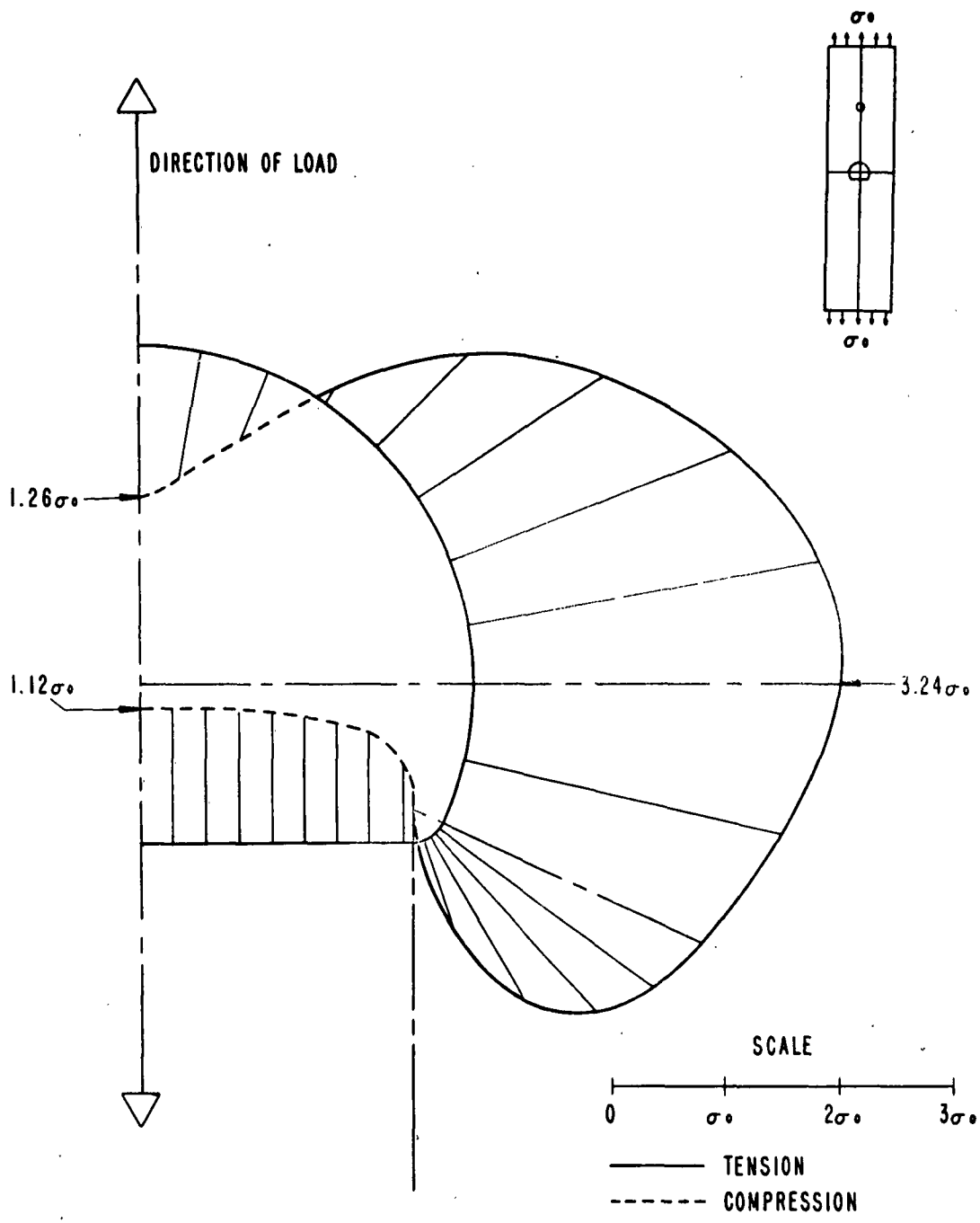

FIG. 13
MODEL 2

IA-6721

IA-6724

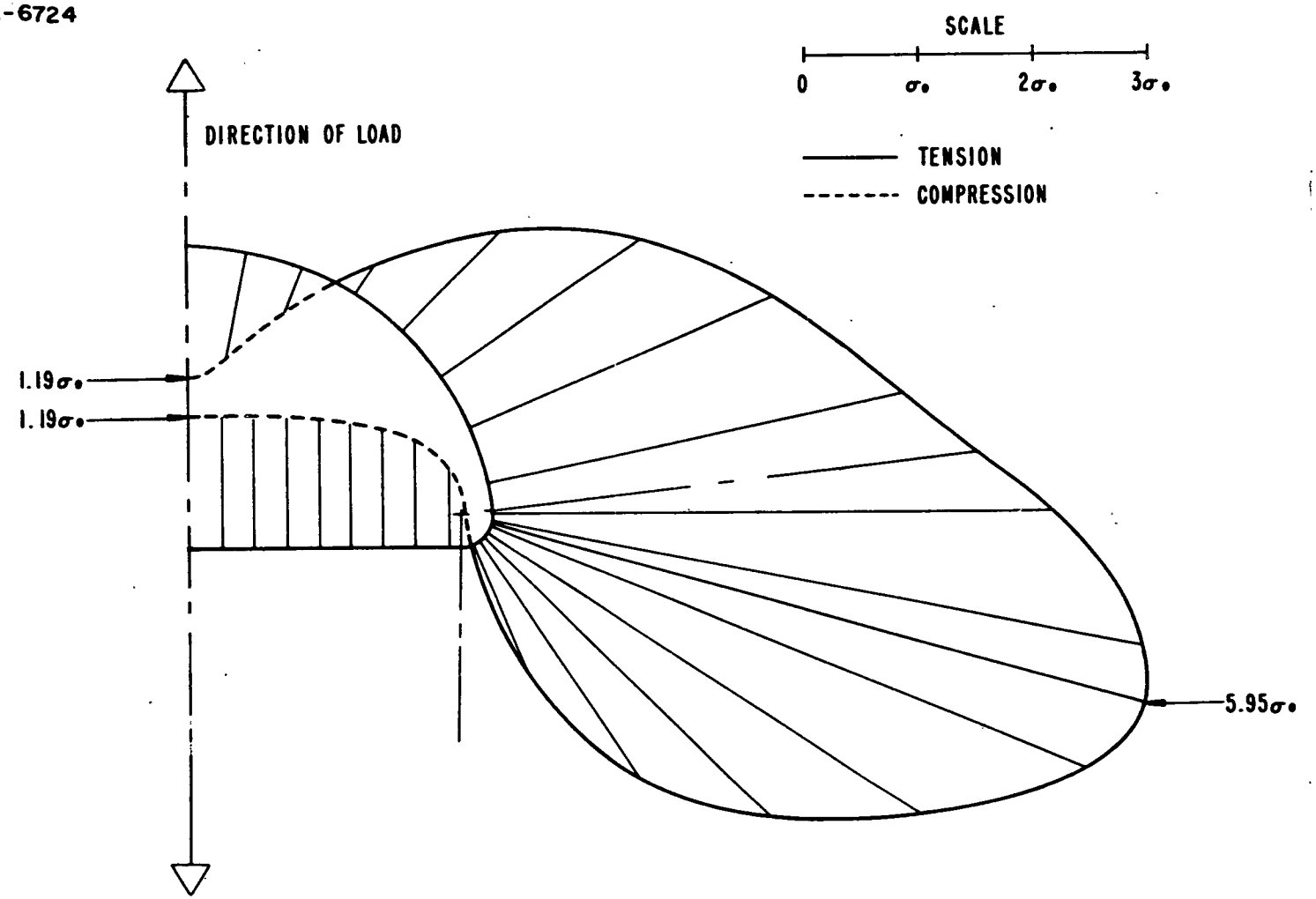

FIG. 14
MODEL 3

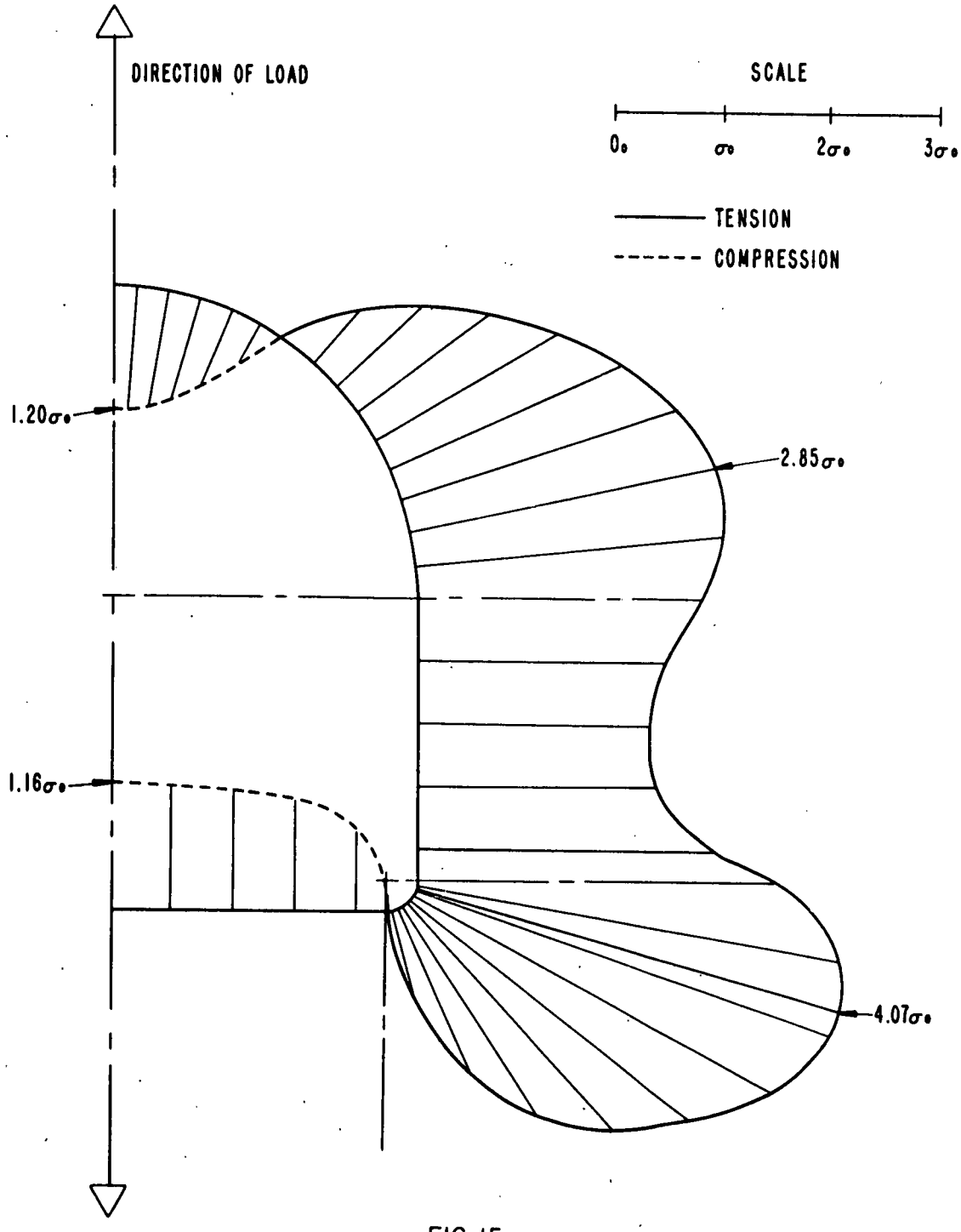

FIG. 15
MODEL 4

IA-6723

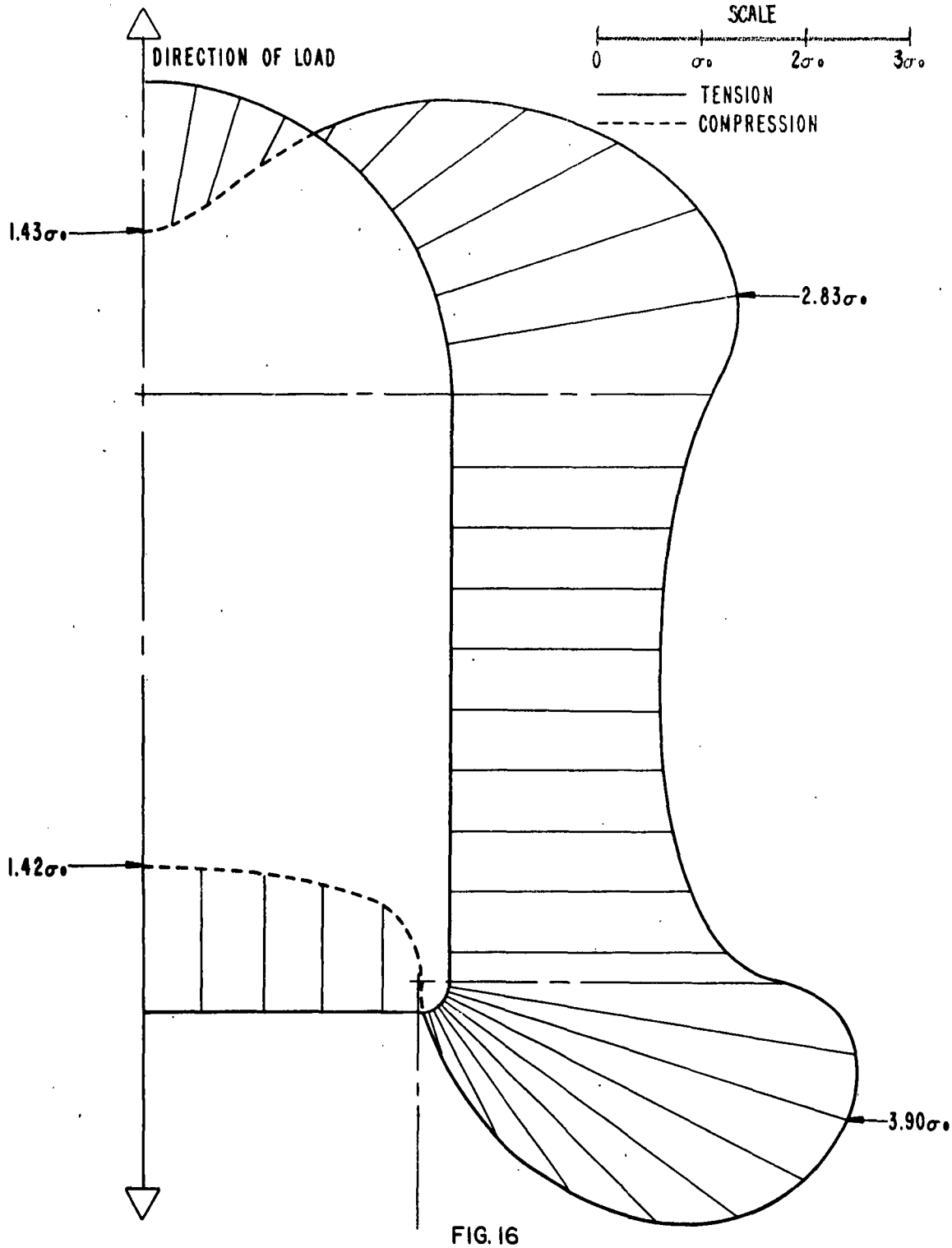

FIG. 16
MODEL 5

IA-6722

IA-6729

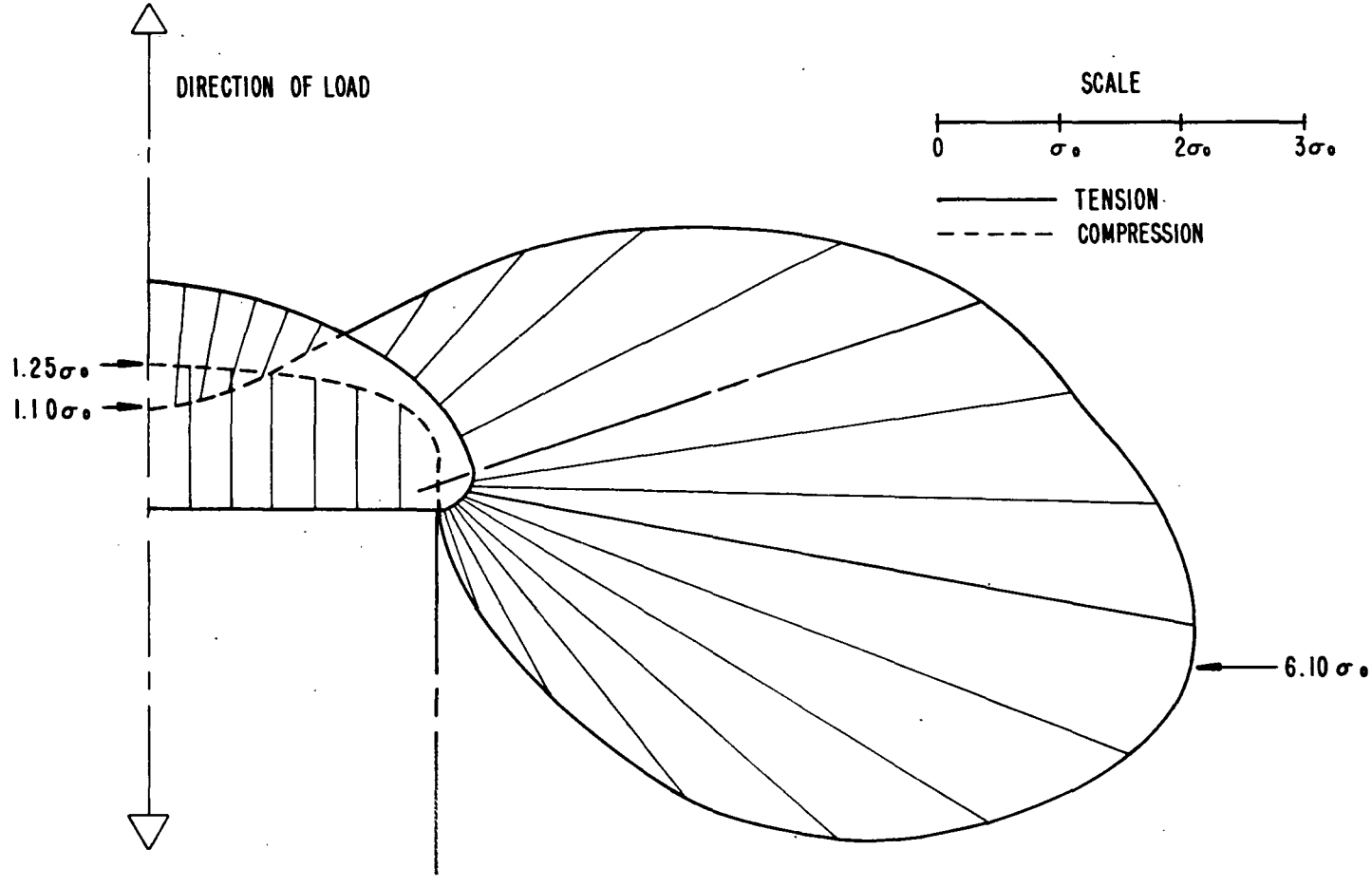

FIG. 17
MODEL 6

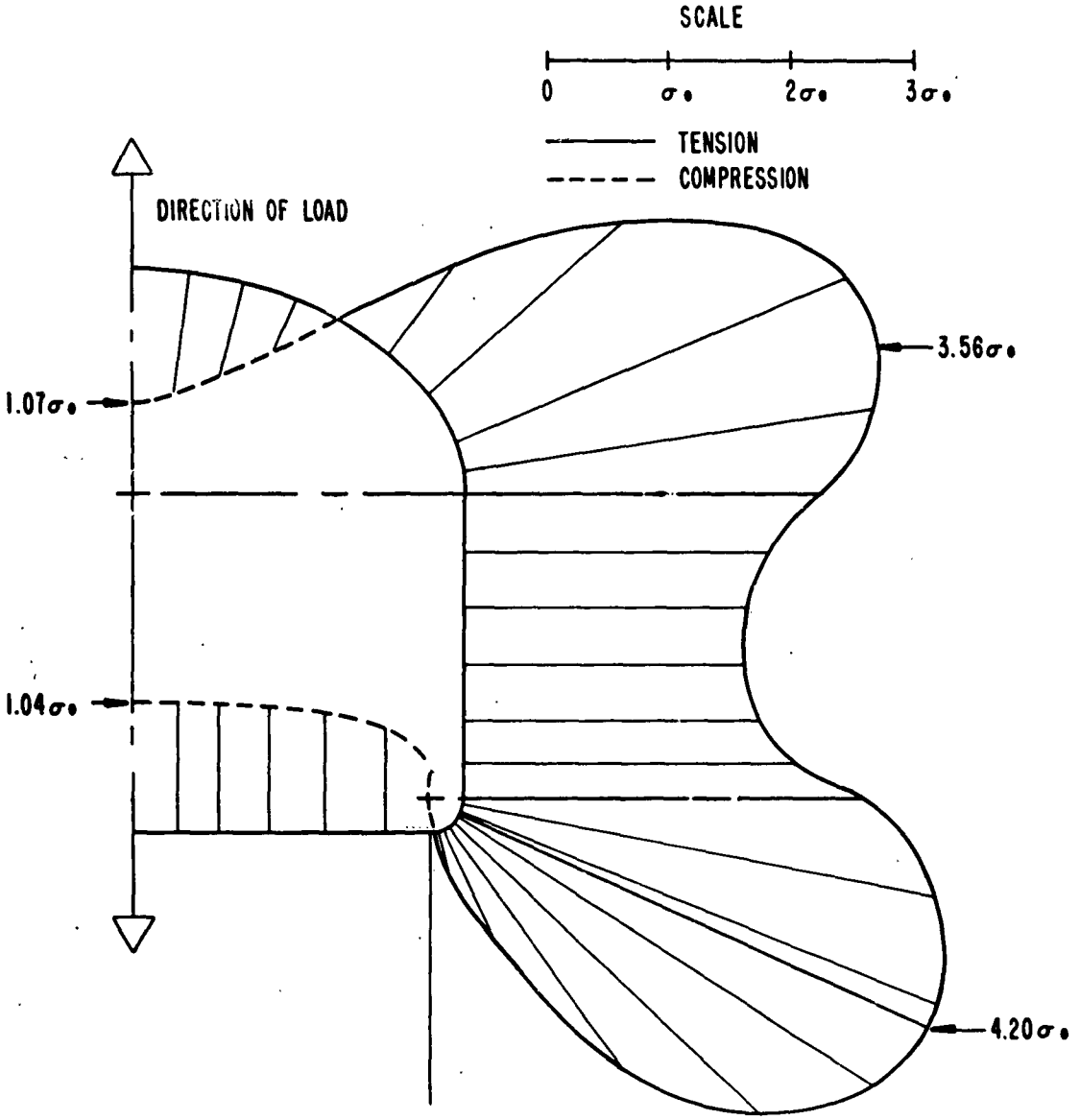

FIG. 18

MODEL 7

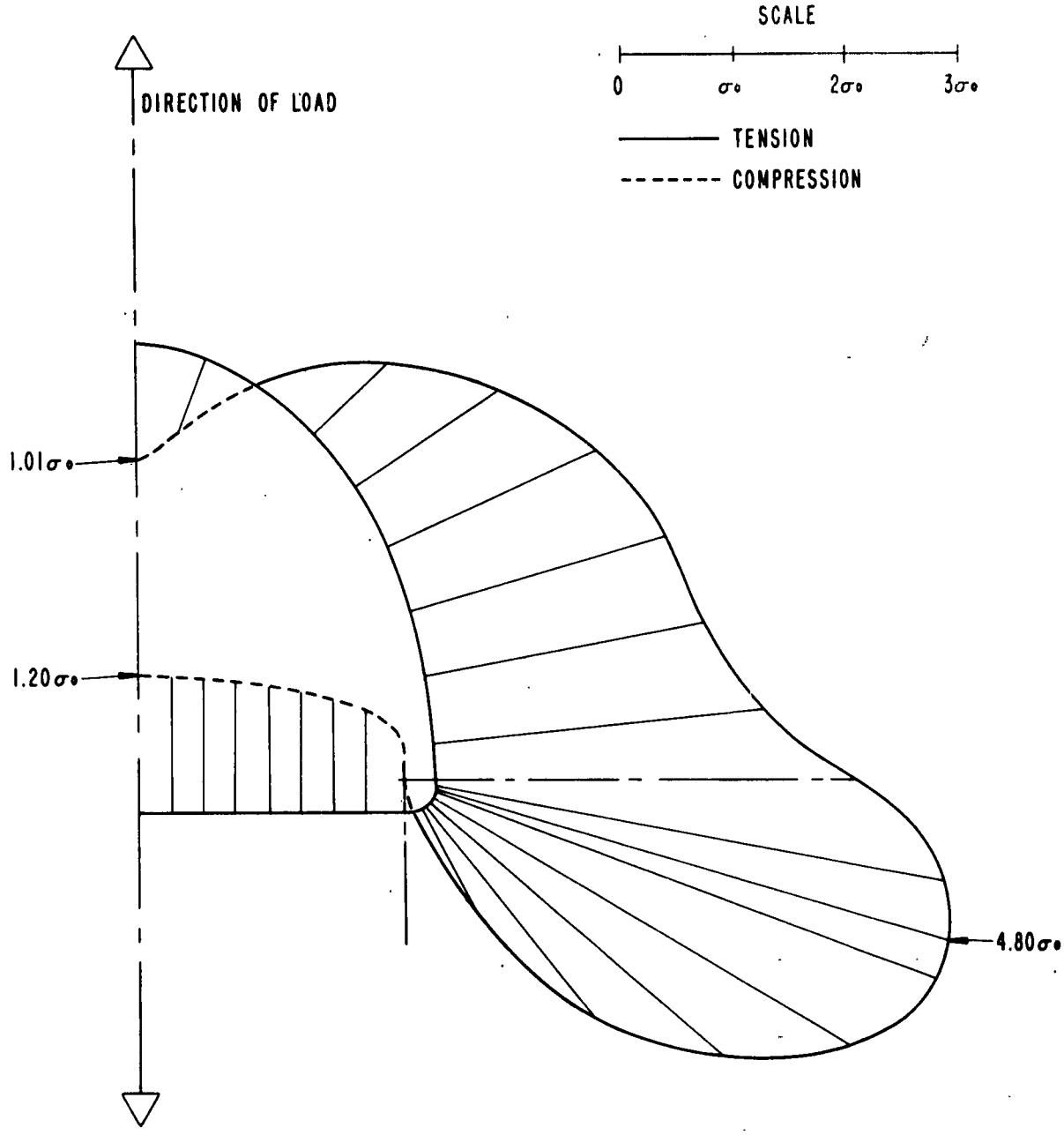

FIG. 19
MODEL 8

IA-6720

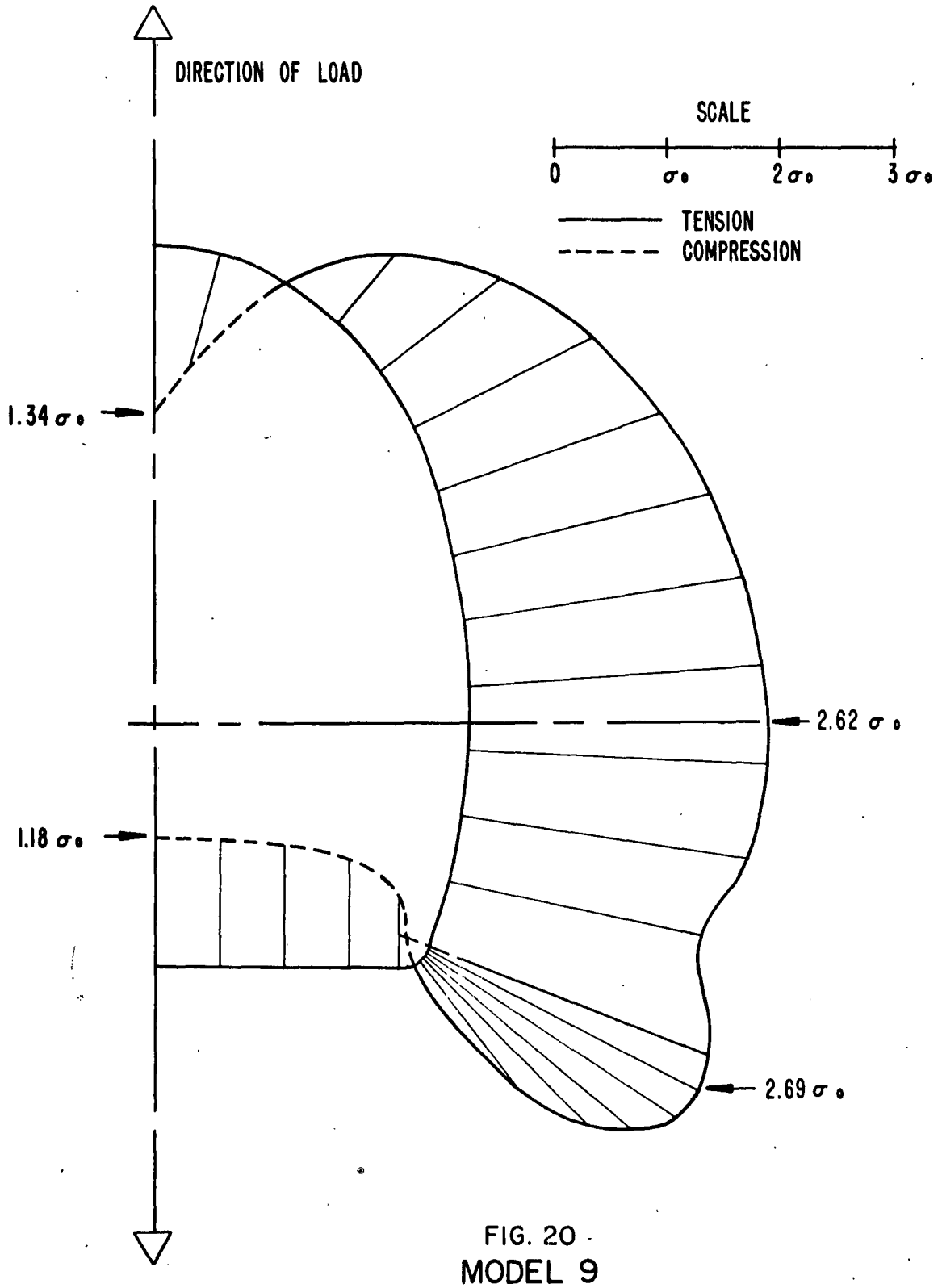

FIG. 20 -
MODEL 9

1A-6725

IB-6719

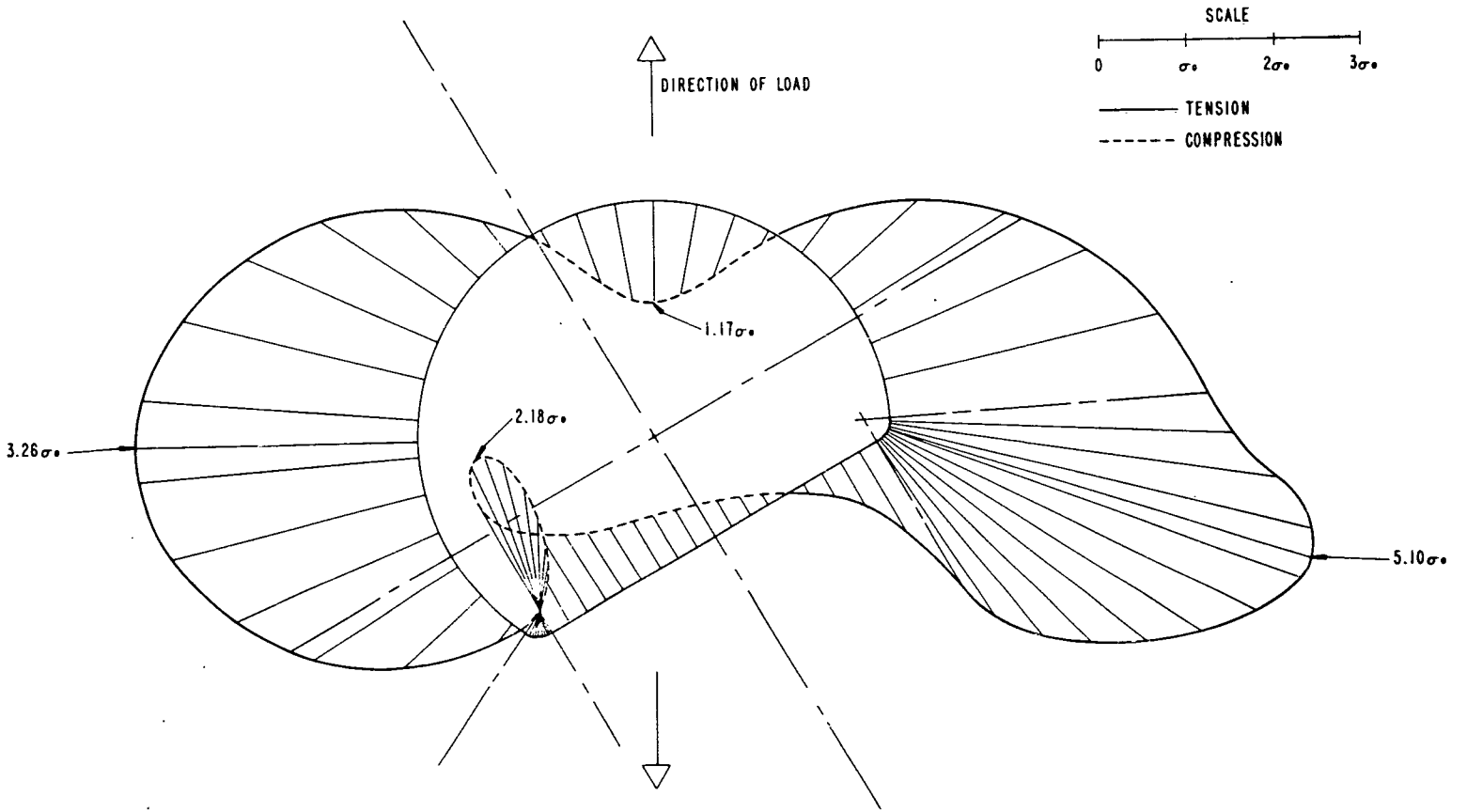

FIG. 21
MODEL 10

TABLE I

TUNNEL CONFIGURATIONS

Model No.	Description
1	Circle
2	3/4 Circle
3	Semi-circle
4	Semi-circle above rectangle, h = r
5	Semi-circle above square
6	Shallow semi-ellipse, $r_1/r_2 = 1.5$
7	Shallow ellipse above rectangle, h = r_1
8	Deep semi-ellipse, $r_1/r_2 = 1.5$
9	3/4 Ellipse (cut at $1.5r_1$)
10	3/4 circle oriented with axis of symmetry 30° from direction of load

h height of rectangle

r radius of circle

r_1 major radius of ellipse

r_2 minor radius of ellipse

Note: Tunnel width held constant at 2 1/2"; 1/8" radius fillets at all corners.

TABLE II

MAXIMUM STRESSES

Spec. No.	Max. Tensile Stress	Max. Compressive Stress
1	$3.24\sigma_o$	$1.36\sigma_o$
2	$3.24\sigma_o$	$1.26\sigma_o$
3	$5.95\sigma_o$	$1.19\sigma_o$
4	$4.07\sigma_o$	$1.20\sigma_o$
5	$3.90\sigma_o$	$1.43\sigma_o$
6	$6.10\sigma_o$	$1.25\sigma_o$
7	$4.20\sigma_o$	$1.07\sigma_o$
8	$4.80\sigma_o$	$1.20\sigma_o$
9	$2.69\sigma_o$	$1.34\sigma_o$
10	$5.10\sigma_o$	$2.18\sigma_o$

BIBLIOGRAPHY

(1) Cratering From a Megaton Surface Burst, H. L. Brode, R. L. Bjork, RM-2600, June 30, 1961, RAND Corporation.

(2) Theoretical Studies on Ground Shock Phenomena, The MITRE Corporation, SR-19, October, 1960.

(3) Stress Wave Phenomena in Semic Solid, W. F. Riley, et al, AFSWC TR-61-25, July, 1961.

(4) Protectective Construction in a Nuclear Age, Edited by J. J. O'Sullivan, "Underground Experience in the Snowy Mountains - Australia", by Thomas A. Lange, Page 688, RAND Corporation, The Macmillan Company, New York, 1961.